Theoretical and Applied Climatology
https://doi.org/10.1007/s00704-020-03183-7

ORIGINAL PAPER

Multi-year analysis of aerosol optical properties and implications to radiative forcing over urban Pretoria, South Africa

Kanike Raghavendra Kumar[1,2] · Richard Boiyo[3,4] · Rehana Khan[2,5] · Na Kang[2] · Xingna Yu[2] · Venkataraman Sivakumar[6] · Derek Griffith[7] · Nulu Latha Devi[1]

Received: 19 June 2019 / Accepted: 8 March 2020

Abstract

The present study focused on investigating the aerosol optical properties and direct aerosol radiative forcing (DARF) using the AERONET Sunphotometer measurements conducted during 2011–2017 over an urban-industrial city, Pretoria (25.75° S, 28.28° E) located in the Northwest of South Africa (SA). Results revealed high aerosol optical depth (AOD_{440}) and Ångström exponent ($AE_{440–870}$) during SON (0.28 ± 0.09, 1.46 ± 0.16) and DJF (0.24 ± 0.07, 1.48 ± 0.18) indicating the dominance of anthropogenic fine-mode aerosols from biomass burning. The single scattering albedo (SSA_{440}) reached a maximum of 0.90 ± 0.05 in DJF and minimum (0.85 ± 0.04) during JJA. The source analysis from the concentration-weighted trajectory (CWT) model exhibited large heterogeneity in all seasons. However, the region is influenced by distinct aerosol types with the abundance of anthropogenic fine absorbing aerosols (86%) and the invisible ratio of dust particles. In addition, the aerosol volume size distribution (VSD) increased with an increasing AOD, exhibiting a bimodal lognormal structure, with a more pronounced peak in fine- relative to coarse-mode particles. Further, the inversion products showed a strong spectral dependence in SSA with substantial heterogeneity in all seasons. At last, the Santa Barbara DISORT Atmospheric Radiative Transfer (SBDART) model showed that the DARF within the atmosphere was more pronounced during SON (46.71 W m^{-2}) and JJA (46.39 W m^{-2}) due to significant differences in AOD and SSA, with an annual mean value of 33.16 W m^{-2}, and the corresponding atmospheric heating rate of 0.96 K day^{-1}. The study provides information on the existing aerosol distribution and their potential impact on climatic change over an urban city in the Northwest of SA and could form a basis for policymaking over the region.

Kanike Raghavendra Kumar and Richard Boiyo contributed equally to this work.

Electronic supplementary material The online version of this article (https://doi.org/10.1007/s00704-020-03183-7) contains supplementary material, which is available to authorized users.

✉ Kanike Raghavendra Kumar
kanike.kumar@gmail.com; rkkanike@kluniversity.in

[1] Department of Physics, Koneru Lakshmaiah Education Foundation (KLEF), Vaddeswaram, Guntur, Andhra Pradesh 522502, India

[2] Collaborative Innovation Centre on Forecast and Evaluation of Meteorological Disasters, Key Laboratory of Meteorological Disasters, Ministry of Education (KLME), Joint International Laboratory on Climate and Environment Change (ILCEC), Key Laboratory for Aerosol-Cloud-Precipitation of China Meteorological Administration, School of Atmospheric Physics, Nanjing University of Information Science and Technology, Nanjing 210044, Jiangsu, China

[3] Department of Physical Sciences, Meru University of Science and Technology, Meru, Kenya

[4] Department of Environment, Energy and Resources, County Government of Vihiga, Maragoli, Kenya

[5] Department of Physics, Higher Education, Government of Khyber Pakhtunkhwa, Peshawar 25000, Pakistan

[6] Discipline of Physics, School of Chemistry and Physics, University of KwaZulu Natal, Durban, KwaZulu Natal 4000, South Africa

[7] Optronic Sensor Systems, Council for Scientific and Industrial Research (CSIR)–DPSS, Pretoria, Gauteng 0001, South Africa

Published online: 21 April 2020

1 Introduction

Atmospheric aerosols, both from natural and anthropogenic sources influence the Earth's radiation budget directly by scattering and absorbing the incoming solar and outgoing terrestrial radiations (Charlson et al. 1992). They also indirectly affect the clouds altering their droplet size distribution and lifetime (Twomey 1977). In addition, they perturb the hydrological cycle (Ramanathan et al. 2001), climate system (Rosenfeld 2000), and human health. The aerosol optical properties (AOPs) including aerosol optical depth (AOD), Ångström exponent (AE), single scattering albedo (SSA), volume size distribution (VSD), and refractive index (RI) are important parameters in controlling the direct aerosol radiative forcing (DARF) at the surface (SFC) and top of the atmosphere (TOA) (Singh et al. 2004; Boiyo et al. 2019). Due to high spatial and temporal variability, the physical and chemical properties of aerosols remain one of the major uncertainties in estimating the climate forcing (IPCC 2013).

In order to get deeper insights into AOPs and their climatic effects, long-term systematic measurements and characterization of aerosols are required. For this, the ground-based remote sensing is ideal for continuous monitoring of column-integrated aerosol properties in different parts of the world. Many global and regional ground-based remote sensing network stations (e.g., Holben et al. 1998; Che et al. 2009) equipped with the Sunphotometer provide various parameters at multiple wavelengths to monitor aerosol properties at relatively high temporal resolution. Unlike satellite products, data from these networks (e.g., Aerosol Robotic Network; AERONET) are not constrained by the aerosol type and surface reflectance because they are based on the measurement of spectral attenuation of direct solar radiation (Bibi et al. 2017; Adesina et al. 2017). A number of studies have been conducted to reduce uncertainties involved in the AERONET data utilizing the measurements from different stations around the globe (e.g., Alam et al. 2012; Kumar et al. 2013; Yu et al. 2017; Che et al. 2015, 2019; Zhu et al. 2019). Apart from this, a number of previous studies established the interesting findings along with the DARF related to dust and biomass burning over different regions in Africa (Piketh et al. 1999; Sivakumar et al. 2010; El-Metwally et al. 2011; Queface et al. 2011; Adesina et al. 2015, 2017; Kumar et al. 2013, 2017; Hersey et al. 2015; Boiyo et al. 2018, 2019).

Over the past few years, the southern part of the African continent, especially South Africa (SA) has experienced an unprecedented increase in aerosol concentrations attributed to the growing population, rapid urbanization, industrialization, and increasing demands for energy (Hersey et al. 2015). The different aerosol sources like dust transported from Namibia, biomass burning from Mozambique and Zambia, sea salt from the Indian and Atlantic Oceans, and industrial-vehicular emissions from distinct sources make the region prone to almost all types of aerosols. It is, therefore, important that continuous and intensive studies of aerosols are carried out to assess the sources, implications, and mitigation measures. Aerosol-related studies over SA (Sivakumar et al. 2010; Adesina et al. 2014; Kumar et al. 2013, 2017; Hersey et al. 2015) have mainly focused on examining the evolution of aerosols on limited temporal scales, except studies by Queface et al. (2011) and Adesina et al. (2017). Keeping the aforementioned need in mind and the lack of long-term analysis, a few studies have devoted in assessing the spatiotemporal distribution of AOPs over SA using satellite observations (Kumar et al. 2014a, Kumar et al. 2015; Adesina et al. 2016). Studies by Queface et al. (2011) reported preliminary results on the AOPs using the long-term AERONET data for Skukuza (in SA) and Mongu (in Zambia) during 1998–2008. Followed this, Kumar et al. (2013, 2014b) conducted an extensive investigation on the AOPs and examined the mechanisms involved in aerosol classification and modification processes with the sun/sky radiometer data over a rural environment of Skukuza (SA) during December 2005–November 2006. Later, Adesina et al. (2014) analyzed the spectral aerosol optical and radiative properties for the year 2012 over Pretoria (SA). They reported significant heating of the atmosphere due to the presence of a large amount of absorbing aerosols over this urban atmosphere. Further, Adesina et al. (2017) demonstrated the impact of fine- and coarse-mode particles on the aerosol VSD and DARF over Skukuza using the AERONET data measured between 1999 and 2010. Recently, Kumar et al. (2017) analyzed the sunphotometry data and examined the impact on DARF in Pretoria during 2011–2015. These authors noticed high AOD during SON and DJF seasons attributed to the dominance of fine-mode particles. In summary, most of these studies have mainly focused on the characteristics of aerosols, source regions, and the role of meteorology, with scarce reports on the implications of climate change. Although these studies laid a strong foundation for aerosol science over the region, they are still limited in terms of analysis techniques, usage, and link with different variables, and/or data span period, and therefore, could not establish a comprehensive characterization of aerosol optical, microphysical, and radiative properties over the region. Hence, there is a need for more complementary and continuous research over the region to understand the ongoing situation of aerosols.

In view of the immense local and regional importance of aerosols and their climatic effects, the present study aims in-depth investigation of the aerosol optical and microphysical properties and radiative forcing over Pretoria in SA, which is an extension to the previous work of Kumar et al. (2017). To accomplish this, we used 7 years (from August 2011 to December 2017) of AERONET data retrieved from the Sunphotometer installed at the campus premises of CSIR_Pretoria over SA. The study overcomes several

objectives that were not fulfilled in our previous works. Specifically, the study focused on the temporal evolution of AOD, source heterogeneity evaluation, the association of column aerosol concentrations with microphysical properties, and classification and modification processes of aerosols that influence the atmospheric dynamics, with implications to radiative forcing from models. In doing so, this study aims at achieving the following objectives: (i) inter-annual changes and spectral dependencies in AOPs, (ii) classification and modification processes of aerosols, (iii) source apportionment studies through the advanced statistical techniques such as concentration weighted trajectory (CWT) methods, and conditional bivariate probability function (CBPF) using the AOD data to identify areas of potential pollution sources, and (iv) DARF computed from well-established global atmospheric radiative transfer models. The rest of this paper is structured as follows: Sect. 2 describes "AERONET site, instrumentation, and methods." "Results and discussions" are elucidated in Sect. 3, while Sect. 4 summarizes the "conclusions" drawn from this research.

2 Site details, instrument, and methods

2.1 Study region and meteorology

The AERONET's observation site named, Pretoria_CSIR_DPSS (25.75° S, 28.28° E, 1449 m above sea level) located in Pretoria over SA (Fig. S1 of Supplementary Material (SM)) has started monitoring the aerosol properties from the beginning of August 2011 to date. Figure S1 of SM presents the topographical map (elevation in m) of SA with its bordering countries and spatial distribution of AOD_{550} derived from the MODIS combined (DT and DB) aerosol product for Aqua observed during the study period over SA. Climatologically, the area experiences a humid subtropical climate characterized by four seasons: DJF (from December to February; DJF), MAM (or fall) (from March to May; MAM), JJA (from June to August; JJA), and SON (from September to November; SON). Most of the observed pollution over SA and its environments originate from large-scale biomass burning (BB) activities that occur during JJA and SON (e.g., Adesina et al. 2017). However, in other seasons like DJF and MAM, the region is predominated with dust and urban/industrial (anthropogenic) pollution (Piketh et al. 1999). In addition to locally produced aerosols, those that are transported remotely from neighboring countries such as Zambia, Zimbabwe, and Mozambique (Queface et al. 2011; Kumar et al. 2013; Adesina et al. 2015) significantly influence the aerosol load. Added to this, the NCEP/NCAR reanalysis data (http://www.esrl.noaa.gov/psd/data) (Fig. S1 of SM) and key meteorological variables (www.wunderground.com) (Fig. S2 of SM) observed from the measurements over SA are presented during January 2011–December 2017. For the detailed discussion on the synoptic meteorology observed over Pretoria, the readers are referred to section S1 of SM and the recently published work of Kumar et al. (2017).

2.2 Instrument and data

The AERONET Sunphotometer of CIMEL Electronique make (Model CE-318) provides three versions and three quality levels of data globally, which is made open to all at http://aeronet.gsfc.nasa.gov/. In this study, we used the Version 2.0 and Level 1.5 (the AERONET did not release the latest Version 3.0 data while began doing analysis) direct sun measurements of AOD retrieved at all multiple wavelengths between 340 and 1640 nm, except at 940 nm, which is used for deriving atmospheric column water vapor content (CWV), and AE computed at different range of wavelengths. Besides these, the level 1.5 inversion products include VSD estimated at 22 radius bins ranging from 0.05 to 15 μm, real (R) and imaginary (I) parts of RI, asymmetry parameter (ASY), SSA, absorption AE (AAE), and extinction AE (EAE) retrieved from the diffuse radiation, which is measured on the almucantar plane at four wavelengths are also used. The summary of data availability and statistics recorded from August 2011 to December 2017 are given in Table S1 of SM. More details on the information related to data acquisition and processing, errors, and uncertainties in the computed AOPs via., AERONET Sunphotometers can be seen in a series of previous works (e.g., Alam et al. 2012; Kumar et al. 2013; Patel et al. 2017; Yu et al. 2017; Boiyo et al. 2019).

2.3 Methods and models

2.3.1 The CWT model

The trajectories arriving at the measurement station were calculated at 500 m above ground level (a.g.l.) for −72 h (backward) using the HYSPLIT (Version 4.0) model of NOAA during the study period at 6-h time intervals (00:00, 06:00, 12:00, 18:00 UTC). The CWT method was performed through the MeteoInfo software with TrajStat Plugin (Wang et al. 2009), which has been proven useful to identify potential source areas of long-range pollution (Zhu et al. 2019). The source area of concern is divided into many small grid cells of equal size. In this method, each grid cell gets a weighted value obtained by averaging the concentration measured at the receptor site as the associated trajectory crosses the grid cell. CWT is calculated as follows:

$$\overline{C_{ij}} = \frac{1}{\tau_{ijk}} \cdot \sum_{k=1}^{n} C_k . \tau_k \quad (1)$$

where C_k is the concentration associated with trajectory endpoints in the ijth cell, and τ_{ijk} is the resident time of trajectory endpoints in the ijth cell. The geographical study area

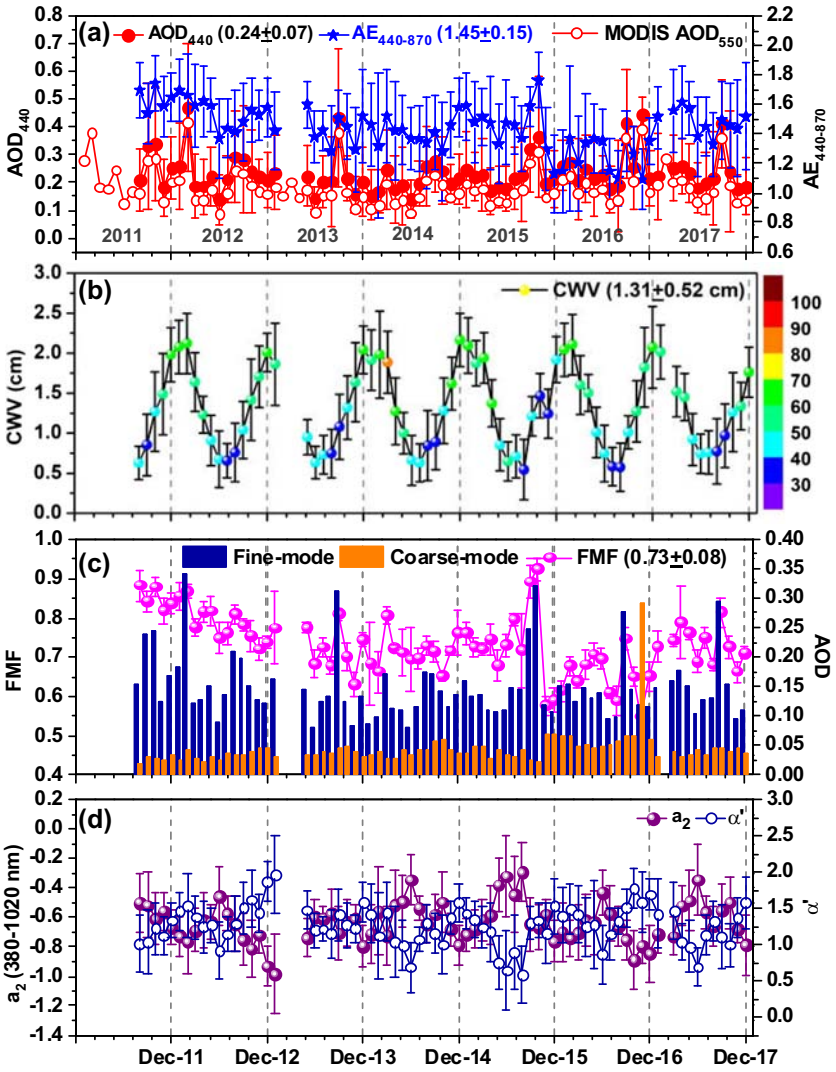

Fig. 1 Monthly time series plots of direct sun products and SDA retrievals at Pretoria. The MODIS merged (DT and DB) AOD550 is also shown in panel (**a**) to correlate with AERONET AOD440; whereas, the CWV is shown as a function of RH. The parameters a2 and α' (=− 2a2) are estimated from the AOD measured in the spectral range between 380 and 870 nm. The vertical lines through the points correspond to the standard deviation of the mean. The annual mean values are also given next to the parameter within parenthesis

identified from 38° to 16° S and 13° to 45° E, covering almost all areas by the air mass transport pathways.

2.3.2 The SBDART model

This study utilized the instantaneous fluxes obtained at TOA and SFC to estimate the DARF in the shortwave (0.3–4.0 μm) region with and without aerosols using the SBDART model and investigated the radiative effects of aerosols. More details concerning the model, its components and sensitivity have been reported by Ricchiazzi et al. (1998), and has been widely used and described well by the previous authors (e.g., Kang et al. 2016; Yu et al. 2016; Patel et al. 2017; Vachaspati et al. 2018; Boiyo et al. 2019). The atmospheric vertical profiles were fixed default by choosing a standard atmosphere in the model as "subtropical." The model output provides the values of upward and downward fluxes at the TOA and SFC which are used to compute DARF and other derived parameters with the necessary equations involved in the computation are given in S3 of SM.

3 Results and discussion

3.1 Direct sun products

3.1.1 Inter-annual changes in AOPs

The multi-year measurements performed by the sunphotometer over urban Pretoria provided an opportunity to examine the changes in intra-annual mean values of AOPs during the study period shown in Fig. 1, whereas Table 1 presents the annual statistics of different aerosol optical and microphysical parameters observed during 2011–2017. Overall, the annual AOD_{440} ranges from 0.14 ± 0.08 to 0.47 ± 0.23, with a mean of 0.24 ± 0.07 during the study period. In general, low AOD (< 0.1) is regarded as clean

Table 1 Inter-annual mean variations of aerosol optical, microphysical, and radiative properties observed in Pretoria. The value next to the mean corresponds to the standard deviation. The respective units for CWV, Vol Con, Eff Rad, DARF, DARFE, and AHR are centimeters, cubic micrometer per square micrometer, micrometer, watts per square meter, watts per square meter per radian, and kelvin per day, respectively, and the rest are dimensionless

Parameter	Inter-annual changes in AERONET direct and inversion products							Annual
	2011	2012	2013	2014	2015	2016	2017	
AOD_{440}	0.214 ± 0.082	0.232 ± 0.072	0.221 ± 0.083	0.205 ± 0.044	0.219 ± 0.062	0.229 ± 0.053	0.231 ± 0.068	0.240 ± 0.069
$AE_{440–870}$	1.521 ± 0.168	1.543 ± 0.121	1.456 ± 0.111	1.459 ± 0.094	1.457 ± 0.166	1.326 ± 0.114	1.472 ± 0.084	1.452 ± 0.151
CWV	1.056 ± 0.502	1.312 ± 0.526	1.201 ± 0.515	1.298 ± 0.509	1.301 ± 0.539	1.330 ± 0.561	1.189 ± 0.425	1.312 ± 0.523
SSA_{440}	0.910 ± 0.027	0.908 ± 0.042	0.896 ± 0.034	0.866 ± 0.041	0.872 ± 0.066	0.752 ± 0.086	0.846 ± 0.031	0.878 ± 0.047
ASY_{440}	0.669 ± 0.007	0.683 ± 0.013	0.684 ± 0.023	0.681 ± 0.021	0.685 ± 0.014	0.694 ± 0.011	0.690 ± 0.013	0.684 ± 0.015
RRI_{440}	1.478 ± 0.037	1.461 ± 0.035	1.476 ± 0.041	1.472 ± 0.039	1.466 ± 0.028	1.483 ± 0.034	1.460 ± 0.024	1.471 ± 0.034
IRI_{440}	0.010 ± 0.003	0.011 ± 0.007	0.013 ± 0.005	0.019 ± 0.008	0.020 ± 0.017	0.066 ± 0.039	0.024 ± 0.007	0.023 ± 0.011
Vol Con-f	0.030 ± 0.011	0.033 ± 0.012	0.029 ± 0.010	0.028 ± 0.006	0.030 ± 0.008	0.028 ± 0.006	0.030 ± 0.007	0.030 ± 0.008
Eff Rad-f	0.130 ± 0.006	0.138 ± 0.009	0.139 ± 0.016	0.135 ± 0.014	0.137 ± 0.009	0.140 ± 0.007	0.137 ± 0.007	0.136 ± 0.010
Vol Con-c	0.035 ± 0.007	0.035 ± 0.008	0.036 ± 0.011	0.038 ± 0.012	0.037 ± 0.010	0.042 ± 0.017	0.047 ± 0.025	0.039 ± 0.014
Eff Rad-c	2.520 ± 0.094	2.484 ± 0.065	2.526 ± 0.103	2.535 ± 0.101	2.480 ± 0.089	2.481 ± 0.087	2.472 ± 0.137	2.499 ± 0.123
$DARF_{SFC}$	− 30.30 ± 11.2	− 31.56 ± 9.28	− 32.66 ± 13.7	− 34.53 ± 11.4	− 35.54 ± 11.7	−51.33 ± 13.5	−37.10 ± 10.3	−36.14 ± 11.58
$DARF_{TOA}$	− 11.31 ± 3.78	− 12.16 ± 3.81	− 11.21 ± 3.06	− 8.37 ± 2.46	− 9.78 ± 4.19	−3.96 ± 4.16	−9.35 ± 2.31	−9.45 ± 3.39
$DARFE_{SFC}$	− 213.9 ± 20.1	− 210.7 ± 33.4	− 218.9 ± 28.5	− 251.8 ± 41.1	− 239.2 ± 53.2	−333.9 ± 66.7	−258.6 ± 21.9	−246.7 ± 37.8
$DARFE_{TOA}$	− 77.89 ± 7.23	− 76.52 ± 12.6	− 73.29 ± 9.55	− 57.37 ± 19.6	− 62.77 ± 25.9	−15.98 ± 31.1	−52.14 ± 10.3	−59.37 ± 16.54
AHR	0.534	0.545	0.603	0.735	0.724	1.332	0.781	0.751

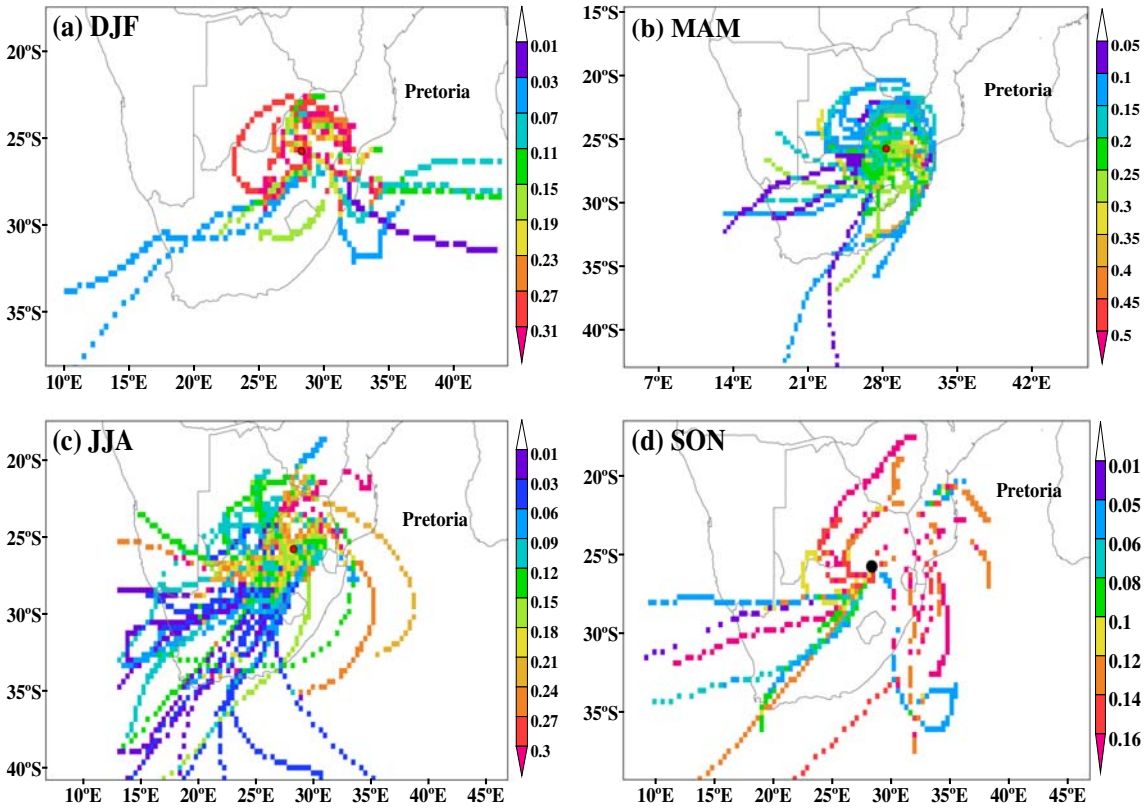

Fig. 2 The CWT spatial maps for AOD_{440} during the study period. The black solid circle in the figure denotes the location of the site

background conditions, while higher (> 0.4) values lead to long-range transport of dust and anthropogenic pollutants (Adesina et al. 2014) over the site. The fluctuations towards higher values of AOD_{440} (> 0.4) appeared in February 2012 and November 2016 attributed to more anthropogenic activities (e.g., biomass burning, transportation and industrial emissions) and dust particles from nearby desert zones. Furthermore, favorable meteorological conditions also result in higher values leading to secondary aerosol formation. In addition, the CWT analysis is performed to identify possible source locations causing AOD variability at the receptor site (Fig. 2). The seasonal mean CWT also revealed a large influence (CWT > 0.3) of potential sources during DJF, and low source influence (CWT < 0.01) during SON. This emphasizes the significant contribution of coarse dust particles originated from the central parts of SA (Kumar et al. 2017). However, the study region experiences aerosols transported predominately from the locally derived relative to long-distance origin. The minimum values of AOD (< 0.2) were found in July of 2012 and 2013 closely related to the shallow atmospheric boundary layer and existing of lower temperatures during the cold winters.

The annual mean AOD measured at Pretoria is generally noticed higher than those found in the rural areas of Africa, like Skukuza (0.22 ± 0.16) in SA during 1999–2010 (Adesina et al. 2017) and Mbita (0.23 ± 0.08) over Kenya from 2007 to 2015 (Boiyo et al. 2018), and also lower than urban Cairo over Egypt (0.64 ± 0.21) as reported by El-Metwally et al. (2011). $AE_{440–870}$ varies between 1.09 ± 0.20 and 1.74 ± 0.19 over Pretoria, with an annual mean of 1.45 ± 0.15 suggesting the particle-size distribution dominated by fine-mode aerosols (Eck et al. 1999). High AOD (> 0.3) and AE (> 1.0) with corresponding large negative values of a_2 (< − 1.0) and positive AE′ (> 1) (Fig. 1d) (also see Fig. S3 of SM) were observed during DJF and SON, implying the dominance of fine-mode particles originated from increased BB activities. Over Pretoria, JJA months are more experienced with cold and dry winters, and AE reaching up to 1.2 which does not favor the secondary production of aerosols. The large variability in both AOD and AE indicates significant heterogeneity with the presence of distinct aerosol types (refer Sect. 4.3 for more details) over the observational site attributed to heterogeneous sources of aerosols.

On the other hand, the annual mean FMF_{500} was found to be 0.9 suggesting a large abundance of fine-mode particles, consistent with the investigations of Adesina et al. (2014) reported at Pretoria measured during 2012. It is revealed that the hygroscopic aerosol growth increases with an increase in relative humidity (RH) and CWV in the atmosphere (Kumar et al. 2013; Adesina et al. 2017) (Fig. 1b). Figure 1c also presents the monthly contributions of fine- and coarse-mode particles on the total AOD at 500 nm for the study period. Obviously, the fine-mode AOD dominated in all months particularly during DJF and SON seasons which are influenced by the meteorological conditions and significant anthropogenic emissions from industries, vehicular transport, biomass burning, and urbanization (Queface et al. 2011). It is also worth noting that the results of fine-mode AOD and FMF obtained from the spectral deconvolution algorithm (SDA) showed a pronounced increase during SON with a maximum in October 2015, revealed the dominance of fine particles produced from BB. However, FMF_{500} varies significantly from 0.5 to 0.95, implying a large variation in aerosol type over the region. The maximum coarse-mode AOD in DJF (December 2016) is mainly due to the presence of regional transported dust and locally generated soil dust or sand particles.

3.1.2 Spectral changes in AOD

To account for the spectral assessment, AOD measured at eight different channels from 340 to 1640 nm was observed during the study period is shown in Fig. 3. Across all the

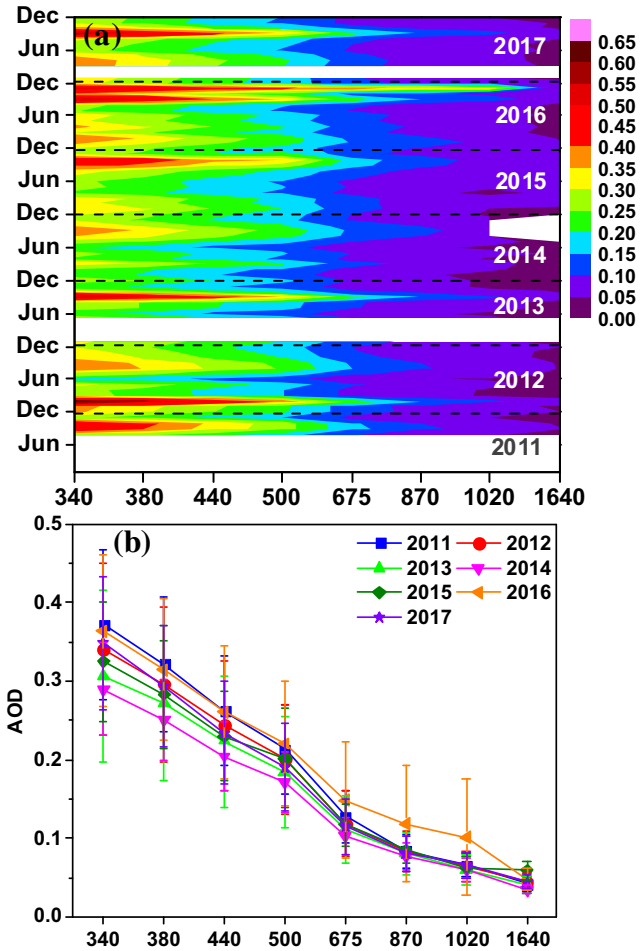

Fig. 3 Temporal and spectral variations of AOD at different wavelengths during the study period. The white color in panel (**a**) indicates data gaps during the study period

panels, it is revealed that AOD decreases with the corresponding increase in the wavelength, indicating systematic spectral dependence (Kumar et al. 2009, Kumar et al. 2013). Higher AOD (> 0.30) at smaller wavelengths are associated with the dominance of fine-mode aerosols as wavelength relates the particle-size, and hence, enhance the scattering and vice versa (Patel et al. 2017). However, the spectral AOD at smaller wavelengths is relatively higher in 2011 followed by 2012 and 2016 (Fig. 2b) presenting high aerosol loading, with an abundance of small-sized particles. It is evident that an abrupt rise in AOD at higher spectral range (from 675 nm onwards) during 2016 indicating the presence of large-size coarse-mode particles. Besides, the seasonal mean AOD showed high values in SON followed by DJF and low during JJA which exhibited a similar pattern in all years round and is closely related to the recent investigations by Kumar et al. (2017).

3.2 Frequency distributions of AOPs

The relative frequency histograms for all the daily averaged AOD_{440}, $AE_{440–870}$, CWV (cm), and SSA_{440} during the four seasons along with their seasonal means and standard deviation are shown in Fig. 4. AOD_{440} exhibited a single mode distribution significantly skewed towards lower values, which is similar to the previous investigations by Queface et al. (2011), Kumar et al. 2013), and Adesina et al. (2014) over SA. It is worth mentioning that all the seasons showed the highest mode in the second-lowest bin interval 0.1–0.2, which is about 35%, 47%, 37%, and 33% to the total during DJF, MAM, JJA, and SON seasons, respectively, suggesting a generally less polluted environment.

Similarly, $AE_{440–870}$ also showed a single peak distribution with skewness on the left side of its distribution, similar to the investigations conducted by Adesina et al. (2014) and Kumar et al. 2013, 2017 over SA. The occurrence of strong mode at a relatively higher size bin (1.6–1.8) supported by seasonal means > 1.0 (Fig. 1a) being more pronounced during DJF and SON seasons implies the dominance of fine-mode particles (Adesina et al. 2014; Kumar et al. 2017). Further, it is shown that the annual mean CWV of 1.33 ± 0.23 cm sequenced in the increasing order of seasons as DJF > SON > MAM > JJA (Fig. 4c). The CWV exhibited the widest unimodal seasonal heterogeneity attributed to complex seasonal patterns of climatic variables. Most of the values were accumulated with CWV > 1.0 cm in all seasons, except during JJA with CWV < 1.0 accounted for 92% (Kumar et al. 2013).

A similar situation has been observed in the case of SSA_{440} with broad distribution values in all the seasons. Besides, the season's JJA and SON peaked at a bin interval of 0.84–0.86, whereas the DJF and MAM seasons peaked at slightly higher bin intervals of 0.96–0.98 and 0.92–0.94, respectively (Fig. 4d). During DJF and MAM, the distribution was dominant at

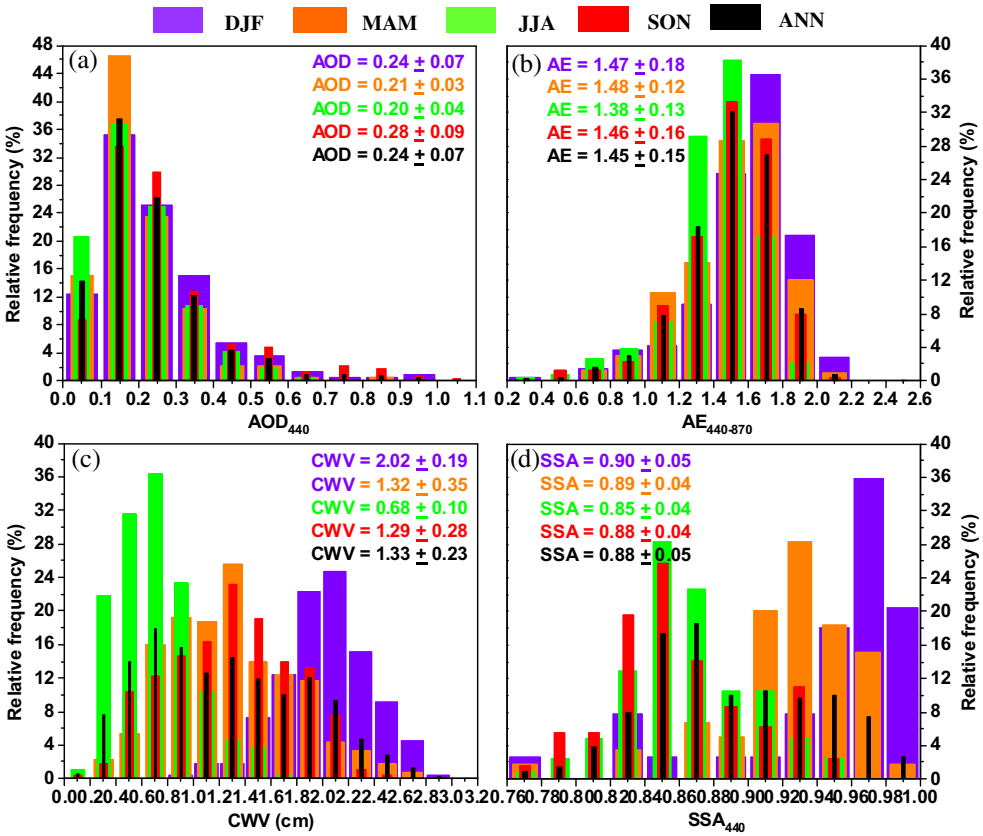

Fig. 4 Relative frequency of occurrences (in %) of AOD440 (**a**), AE440–870 (**b**), CWV (**c**), and SSA440 (**d**) for four seasons. The respective mean (±•) values for the annual and individual seasons are also given inside the panel. The number within the parenthesis corresponds to the number of days of observations

higher values of SSA_{440} (> 0.9) accounted for 79% and 82%, respectively, suggesting more amount of scattering particles in the atmosphere. Whereas, the maximum SSA_{440} values in JJA and SON were accumulated from 0.82 to 0.88 with the contribution of 75% and 72% of the total, respectively (Fig. 4d). This signifies that generally the polluted environment is dominated by absorbing aerosol type rather than scattering type.

3.3 Aerosol types and classification mechanisms

3.3.1 Aerosol modification process

Following Gobbi et al. (2007) (more details are given in S5 of SM), we have demonstrated the modification of aerosol properties using $AE_{440–870}$ and difference in AE (dAE = $AE_{440–675}$ − $AE_{675–870}$) (Fig. 5) as a function of AOD at 675 nm (AOD_{675} > 0.15 were only allowed) represented by different colors of increasing turbidity. The seasonal scatter plots of $AE_{440–870}$ versus dAE exhibited similar patterns during four different climatic seasons, signifying the dominance of either fine- or coarse-mode particles over the study site (Fig. 5). Low values of AOD_{675} found outside the classification scheme leading to some errors in the estimation of $AE_{440–870}$ and dAE, as well as uncertainties while measuring AOD_{675} (Kaskaoutis et al. 2011). It is evident from Fig. 5 that the majority of data points with high AOD_{675} (> 0.4) in all seasons at Pretoria were associated with high $AE_{440–870}$ (> 1.2), dAE < 0 and η > 70%, being more pronounced during SON and DJF and least during MAM and JJA. This indicates that the high turbidity conditions over the region are associated with the dominance of fine-mode aerosols likely due to biomass burning and urban-industrial emissions. The increase in AOD takes place perpendicular to the R_f curves (from ~ 0.15 to ~ 0.18 μm) interpreting the coagulation of fine particles under turbid atmospheres (Patel et al. 2017). Similar modifications in η and R_f for increasing AOD are reported in a number of previous studies including Kaskaoutis et al. (2011), Kang et al. (2016), Patel et al. (2017), and Yu et al. (2017) over different environments. However, investigations by Boiyo et al. (2018) reported that the increase in AOD took place along the R_f curves attributed to cloud contamination. It can, therefore, be inferred that high AOD at Pretoria may be

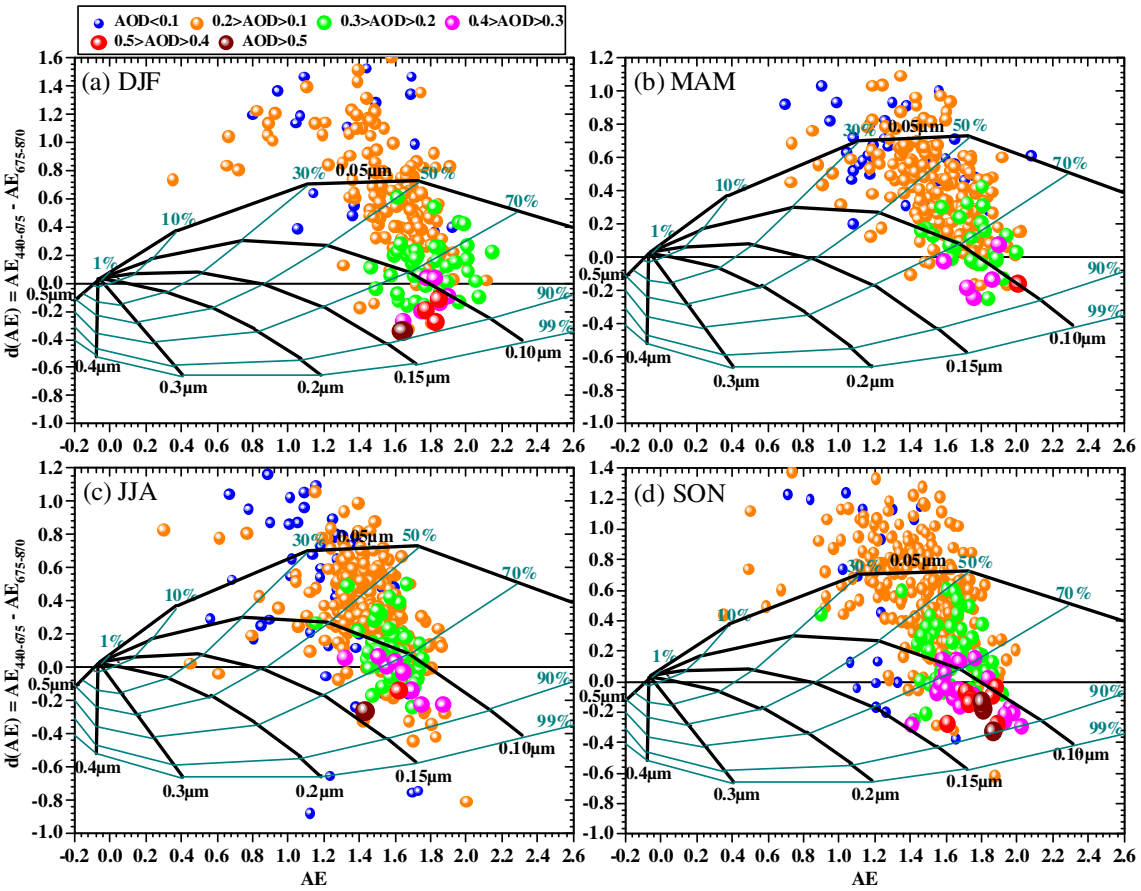

Fig. 5 Ångström exponent difference, dAE = AE (440–675 nm) − AE (675–870 nm) as a function of AE (440–870 nm) and AOD675 (colored data points representing different AOD bin size) for bimodal and log-normal size distributions observed over Pretoria in different seasons. The black lines indicate the fixed effective radius (*Rf*) of the fine mode and the cyan lines for the fixed fraction (η) of fine mode to the AOD at 675 nm. Increase of the colored circle symbols denotes increase in AOD

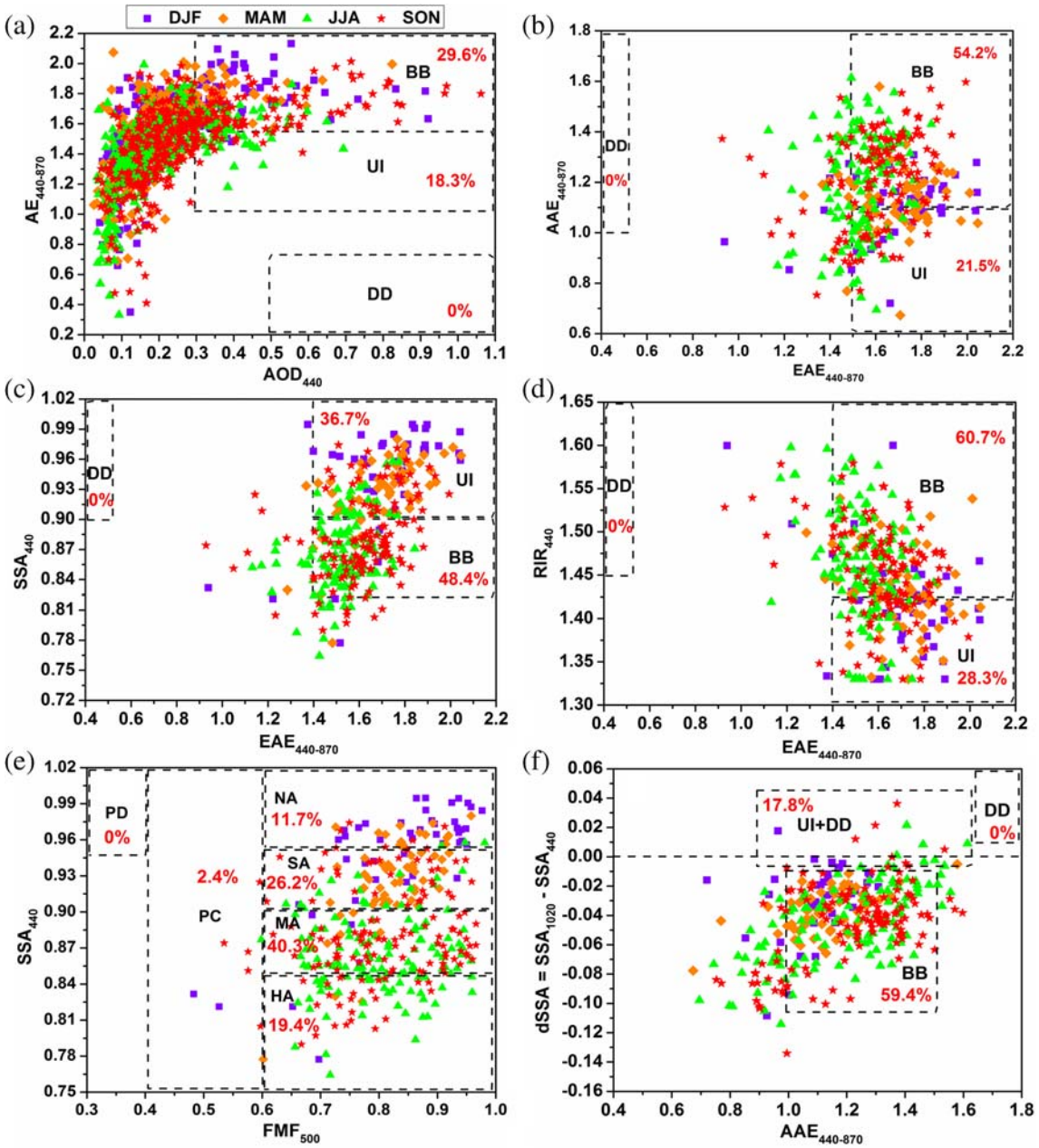

Fig. 6 Seasonal scatter plots between different aerosol optical properties to discriminate dominant aerosol types with their percentage contributions at Pretoria. The representations of aerosol types are mentioned in the text, with their threshold values are given in Table 2

associated with increased concentration of fine-mode particles which coagulate under high turbid conditions.

3.3.2 Discrimination of aerosol types

The classification of major aerosol types such as biomass burning (BB), urban/industrial (UI), and desert dust (DD) is needed due to their distinct sources, and can be discriminated by adopting several clustering techniques (refer S6 of SM) (Bergstrom et al. 2007; Kaskaoutis et al. 2007; Russell et al. 2010; Lee et al. 2010; Bibi et al. 2016; Boiyo et al. 2019). The identification of these aerosol types from their mixture and their contributions (in %) are given in Fig. 6. The threshold values used in the AOD-AE method to identify dominant aerosol types are given in our recently published work (Kumar et al. 2017), and hence not repeated as the study site is the same. The scatter plots of $AAE_{440–870}$ versus $EAE_{440–870}$, drawn on a seasonal basis, with their thresholds given in Table 2, are shown in Fig. 6. It is revealed that the BB aerosol type made the highest contribution followed by UI type. The BB type is characterized by higher AAE values due to increased OC fraction, while UI refers mostly to BC from fossil-fuel (AAE around 1) and mixtures of inorganic species (i.e., ammonium, sulfate, nitrate, chloride) (Katsanos et al.

Table 2 Threshold values used to define different aerosol types for the aerosol optical properties observed over Pretoria

Aerosol type	EAE Vs. AAE		EAE vs. SSA		EAE vs. RIR	
UI	EAE > 1.4	AAE < 1.1	EAE > 1.4	SSA > 0.9	EAE > 1.4	RIR < 1.42
BB	EAE > 1.4	AAE > 1.1	EAE > 1.4	0.82 < SSA < 0.9	EAE > 1.4	RIR > 1.42
DD	EAE < 0.5	AAE > 1.0	EAE < 0.5	SSA > 0.9	EAE < 0.5	RIR > 1.45

2019). Following the same, we observed the similar dominance of BB aerosol type over UI from the scatter plots between SSA_{440} versus $EAE_{440–870}$, and RIR_{440} versus $EAE_{440–870}$ over the study region. However, the two optical parameters do not have the potential impact on aerosol discrimination such as absorbing and non-absorbing aerosols (Lee et al. 2010; Giles et al. 2012; Russell et al. 2010). Similarly, it is evident from the relationship of dSSA (SSA_{1020}-SSA_{440}) versus $AAE_{440–870}$ that the BB type ($1 < AAE_{440–870} < 1.5$, $dSSA < 0$) constituted the dominant aerosol type at Pretoria, followed by UI ($0.9 < AAE_{440–870} < 1.6$, $dSSA > 0$) (Fig. 6f). In contrast, all the techniques showed a complete absence of DT aerosol at the site mainly attributed to enhanced mixing processes into the urban environment as well as suppressed emission of dust particles. This is not the case because the CWT analysis showed the possibility of transported dust plumes from the desert environment in the west and north parts of SA.

To discriminate absorbing and non-absorbing aerosols, the daily mean data of FMF_{500} and SSA_{440} is presented as a scatter diagram shown in Fig. 6e and thresholds used are discussed in S6 of SM. It is evident from Fig. 6e that FMF_{500} varied from 0.45 to 0.98 characterizing the predominance of fine- relative to coarse-mode, while SSA_{440} was recorded between 0.76 and 0.99 at the study site. Overall, the fine-mode aerosol types were disintegrated as polluted

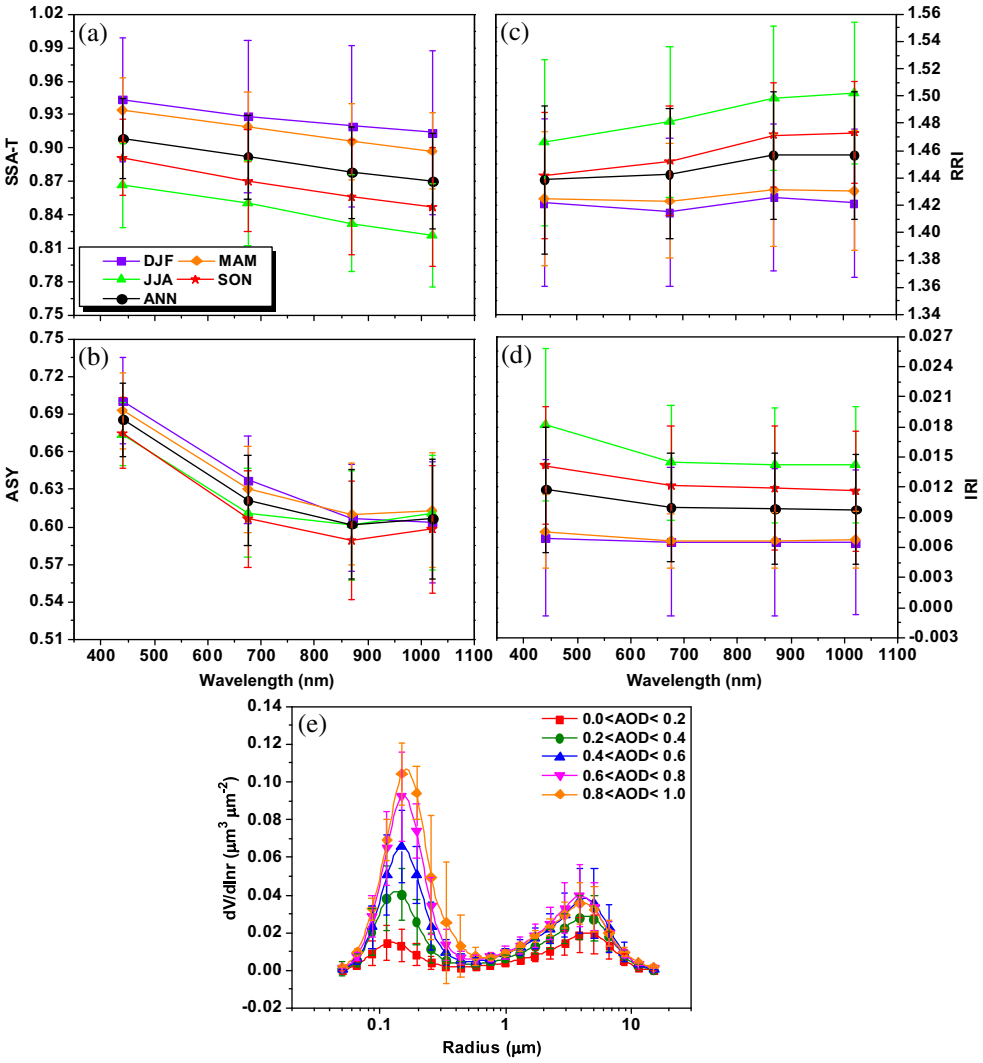

Fig. 7 **a**–**d** Seasonal spectral variations of almucantar retrieved inversion products observed at Pretoria. **e** Variations of aerosol volume size distribution for different AOD440 observed at Pretoria during the study period

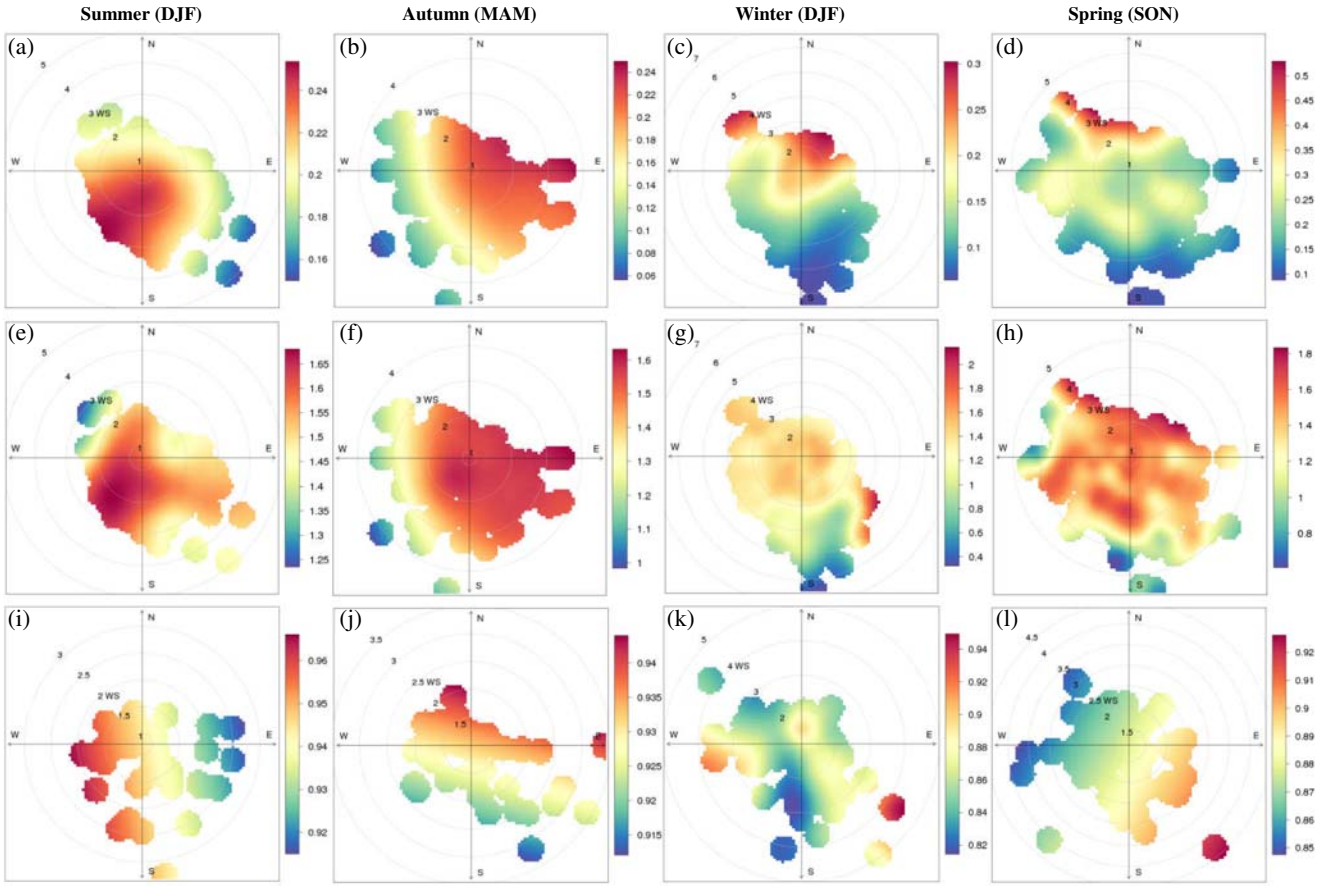

Fig. 8 Seasonal bivariate plots for AOD440 (**a**–**d**), AE440–870 (**e**–**h**), and SSA440 (**i**–**l**) with respect to wind speed and direction observed at Pretoria

continental (PC; background aerosols), polluted dust (PD; dust mixed with anthropogenic aerosols), non-absorbing (NA; organic and inorganic aerosols), and absorbing aerosols, which constitute black carbon are further classified as slightly absorbing (SA), moderately absorbing (MA), and highly absorbing (HA) and their respective annual contributions were found to be 2.4%, 0%, 11.7%, 26.2%, 40.3%, and 19.4%. However, the negligible contribution of PD type is due to enhanced precipitation in DJF (Fig. S2 of SM) that suppresses the emission of coarse dust particles. In contrast, the highest contributions of absorbing type aerosols with a maximum of MA (40.3%) were noticed as a result of aerosols produced from local anthropogenic activities (industries, national highways, agriculture, and biomass burning) and secondary aerosol formation at Pretoria.

3.4 Changes in almucantar inversion products

The spectral variations of optical parameters obtained from the almucantar retrievals at Pretoria during the measurement period are shown in Fig. 7 a and b. It is evident that both the SSA and ASY are spectral dependent, where the SSA decreases with wavelength for the BB and UI type of aerosols. Further, an increased presence of BB (a large fraction of OC aerosols) enhances the decreasing rate of SSA (Patel et al. 2017; Katsanos et al. 2019). There is a strong absorption at higher wavelengths resulting in low SSA, due to the interaction of soil dust particles with the incoming solar radiation (Singh et al. 2004; Boiyo et al. 2019). However, an increase in SSA (> 0.9) and ASY at the regular spectral range during DJF (low Real-RI, Fig. 7c and S7 of SM) suggesting an abundance of anthropogenic aerosols likely related to the effect of water-soluble aerosols under high CWV (Singh et al. 2004). While the decrease in SSA (0.8–0.9) and ASY was observed in SON significantly indicating that the region is highly accumulated with anthropogenic absorbing aerosols from biomass burning and/or forest fires. In contrast, the respective lower and higher values of SSA and RII (imaginary-RI) (Fig. 7d and S7 of SM) during JJA were generally associated with strong absorption by anthropogenic black/organic carbon from biomass burning. Further, it is revealed that there is an increased absorption at 440 nm with negative Δ_{SSA} (SSA_{440}-SSA_{1020}) for $AE_{440–870} < 1$ (S8 and Fig. S5b of SM) implies significant absorption due to a mixture of dust aerosols. However, the extremely low values of Δ_{SSA} (< − 1) suggest the dominance of iron oxides likely from dust aerosols (Derimian et al. 2008).

The VSD was studied as a function of AOD_{440} to show the relationship between the fine- and coarse-mode aerosols (Fig.

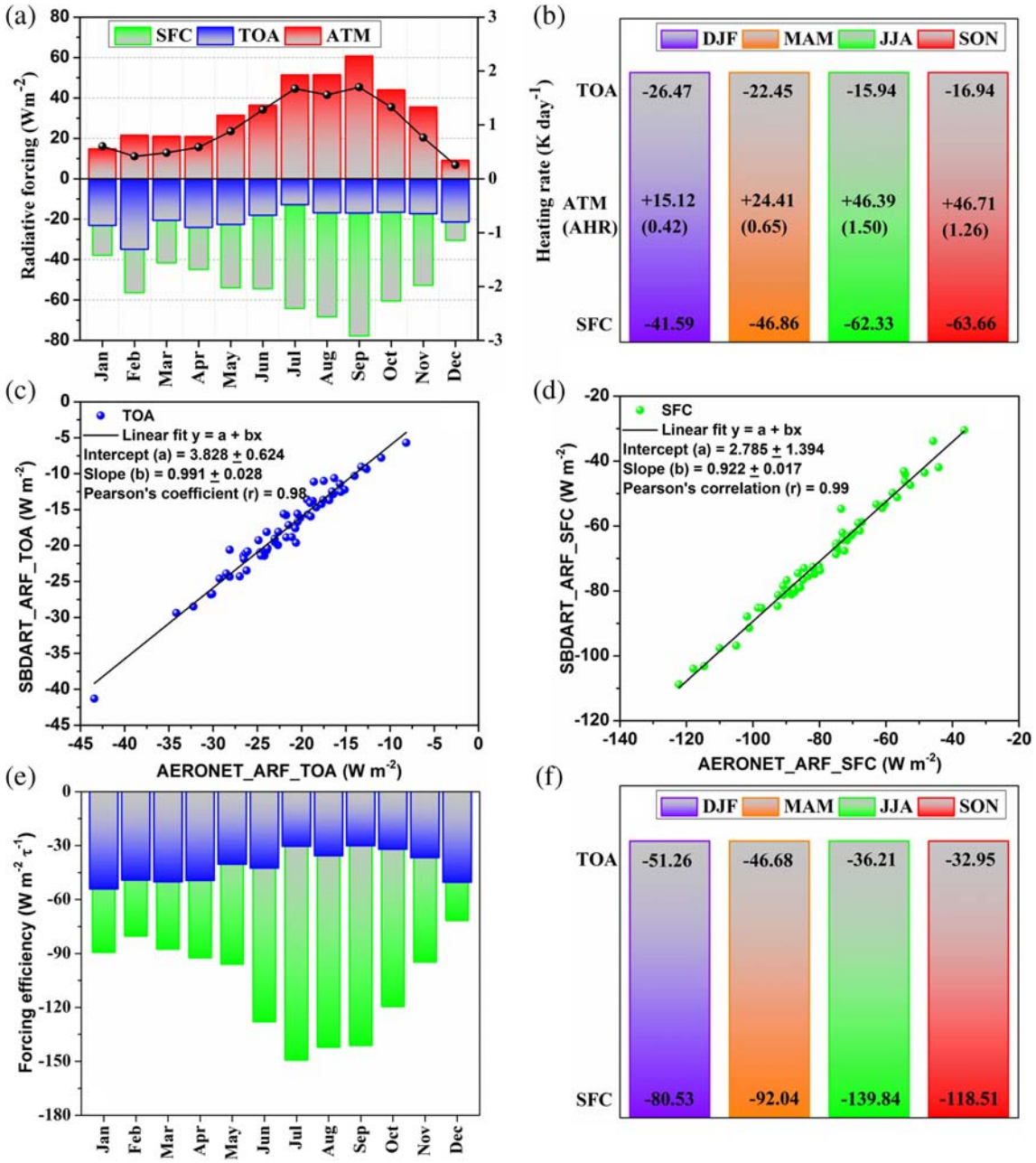

Fig. 9 Monthly and seasonal changes of SBDART model derived direct aerosol radiative forcing (**a**, **b**) and its efficiency (**e**, **f**) at TOA, SFC, and ATM at Pretoria for the study period. The atmospheric heating rates for the corresponding ATM forcing are shown with a solid black line in panel (**a**) and within the parenthesis in panel (**b**). The regression statistics and correlation coefficient (*r*) between AERONET and SBDART derived ARF are also given in panels (**c**, **d**) computed at the (**c**) TOA and (**d**) SFC

7e). It is obvious that the VSD patterns noted at Pretoria exhibited a bimodal distribution with fine-mode peaked at a radius of 0.15 μm and coarse-mode around 3.86 μm (Fig. 7e). The noticeable fact is that there is a significant increase in fine-mode volume concentration with increasing AOD, implying mainly the dominance of fine-mode particles. Notably, for low AOD_{440} (< 0.2) the difference in aerosol volume concentration for fine- and coarse-modes is small. However, for large AOD_{440} (> 0.3), the aerosol volume concentration in fine-mode is predominantly large, obviously visible during SON attributed to increased anthropogenic BB activities at Pretoria.

3.5 Influence of wind speed and direction on AOPs

The bivariate polar plot, a technique used to identify the source and characterizing the relationship between the variables used was implemented in this study making use of wind speed and direction. The season-wise bivariate plots show the mean concentrations of AOD_{440}, $AE_{440–870}$, and SSA_{440} for

the study period observed at Pretoria (Fig. 8). Low to moderate wind speeds (> 3 ms^{-1}) blowing from the northern directions during DJF and MAM resulted in higher aerosol loading (Fig. 8a). A recent study by Hersey et al. (2015) also found a higher value of AOD during the DJF due to the weak wind speeds (< 2 ms^{-1}) coming from the north direction over SA. In contrast, all the seasons revealed the dominance of fine-mode particles produced from local anthropogenic and biomass burning emissions at low wind speed (< 2 ms^{-1}) from all directions, which does not favor the dispersion processes. However, distinct features were observed in SSA for each season with a similar pattern as observed in AOD. It is revealed that the SSA varies with the direction depending on the seasons. The maximum was found when the winds were blowing from the north at > 3 ms^{-1} indicate more scattering type rather than absorbing aerosols.

3.6 Radiative forcing: model versus AERONET

Figure 9 features the aerosol radiative effects both at the TOA and SFC, and the corresponding efficiencies observed at Pretoria during the study period. The monthly and seasonal mean values of DARF averaged for all the years, together with the validation results are shown in Fig. 9 a and b. A strong correlation was observed at TOA (0.98) and SFC (0.99) between the DARF estimated using the SBDART and that of the ones derived from AERONET (Fig. 9 c and d). The monthly mean DARF estimated at the TOA, SFC, and ATM during 2011–2017 varied from − 34.20 to − 12.88 W m^{-2}, − 77.72 to − 30.47 W m^{-2}, and 9.07 to 60.74 W m^{-2}, respectively. In contrast, the AHR ranged from 0.25 to 1.70 K day^{-1}, with a mean value of 0.96 ± 0.52 K day^{-1} (Fig. 9a). The seasonal mean values of $DARF_{ATM}$ were found to be 15.12 W m^{-2}, 24.41 W m^{-2}, 46.39 W m^{-2}, and 46.71 W m^{-2} during DJF, MAM, JJA, and SON, respectively (Fig. 9b). Further, high values of forcing in the atmosphere were observed during SON (46.71 W m^{-2}) followed by JJA suggesting a large abundance of absorbing aerosols (mostly biomass burning) characterized by higher values of AOD and lower values of SSA. The corresponding monthly mean DARFE ranged from − 149.32 to − 71.75 Wm^{-2} τ^{-1} (SFC) and − 54.15 to − 30.15 Wm^{-2} τ^{-1} (TOA), with respective mean values of − 107.73 ± 26.81 and − 41.77 ± 8.72 W m^{-2} τ^{-1} (Fig. 9e, f) during 2011–2017 over Pretoria.

4 Conclusions

Using the 7 years (January 2011–December 2017) of ground-based AERONET measurements combined with model simulations, the study presented an in-depth assessment of column-integrated aerosol optical, microphysical, and radiative properties over an urban environment (Pretoria) in the Northwest of South Africa. The findings extracted from this study have provided vital information regarding aerosols properties and its radiative effects are summarized as follows:

1. The annual mean AOD_{440} (0.24 ± 0.07), with a single-mode distribution peak, was noticed higher during SON (0.28 ± 0.09) followed by DJF (0.24 ± 0.07), and lower during JJA (0.20 ± 0.04) and MAM (0.21 ± 0.03) seasons. In contrast, the annual mean $AE_{440–870}$ (1.45 ± 0.15) was found more pronounced in DJF (1.47 ± 0.18) and SON (1.46 ± 0.16) and relatively low during MAM and JJA seasons.
2. The closer investigation on absorbing aerosols (BB type) revealed the highest loading during DJF and SON attributed to enhanced biomass burning activities. The aerosol modification process indicated an increase in AOD took place perpendicular to the R_f curves (from ~ 0.15 to 0.18 μm), clarifying the coagulation of fine-mode particles under turbid atmospheres.
3. The annual mean SSA_{440} (0.88 ± 0.05) showed the highest values during DJF followed by MAM, and lowest values during JJA and SON seasons. However, the low SSA_{440} in SON (0.84) is attributed to the dominance of fine-mode absorbing aerosols resulting from increased biomass burning.
4. The VSD exhibited bimodal lognormal structure with a geometric mean radius of 0.15 μm and 3.86 μm for fine and coarse modes, respectively, with a higher volume concentration of 0.105 μm^3 μm^{-2} in the fine-mode for maximum AOD due to the buildup of anthropogenic aerosols.
5. In spite of the differences in methodology and algorithms for radiative transfer and uncertainties in the input variables, the values of DARF simulated from the SBDART model were in good agreement with the AERONET derived values at the TOA and SFC, evidenced by high correlations of 0.98 and 0.99, respectively. The annual mean values of SFC, TOA, and ATM forcing were found − 20.45 ± 5.62 W m^{-2}, − 53.61 ± 13.37 W m^{-2}, and 33.16 ± 16.27 W m^{-2} over Pretoria during 2011–2017, with an atmospheric heating rate of 0.96 ± 0.52 K day^{-1}.

The findings in this study can not only serve as an up-to-date reference database for future field measurements and modeling work but are also expected to be beneficial for policymakers to retrofit air pollution control strategy in this region, if necessary in time.

Acknowledgments We owe our sincere thanks to the Principal Investigator, Prof. Brent Holben, and his staff for establishing and maintaining the AERONET station, as well as other data sources used in this study. Thanks are due for procuring the NCEP/NCAR data at http://www.esrl.noaa.gov/psd/data and meteorological variables from the Weather Underground website (www.wunderground.com). The authors would

like to acknowledge Prof. Hartmut Graßl, Editor-in-Chief of Theoretical and Applied Climatology Journal, and the anonymous reviewers for their helpful comments and constructive suggestions towards the improvement of an earlier version of the manuscript.

Funding information This work was supported by the National Natural Science Foundation of China (Grant Nos. 41805121, 41775123, 91644224) and the National Research Foundation (NRF-South Africa) bi-lateral research grant (UID: 78682). The authors (KRK and NLD) thanks the Department of Science and Technology (DST), Govt. of India for the award of DST-FIST Level-1 (SR/FST/PS-1/2018/35) scheme to the Department of Physics, KLEF, India.

Compliance with ethical standards

Conflict of interest The authors declare that they have no conflict of interest.

References

Adesina AJ, Kumar KR, Sivakumar V, Griffith D (2014) Direct radiative forcing of urban aerosols over Pretoria (25.75°S, 28.28°E) using AERONET Sunphotometer data: first scientific results and environmental impact. J Environ Sci 26:2459–2474

Adesina AJ, Kumar KR, Sivakumar V (2015) Variability in aerosol optical properties and radiative forcing over Gorongosa (18.97°S, 34.35°E) in Mozambique. Meteorog Atmos Phys 127:217–228

Adesina AJ, Kumar KR, Sivakumar V, Piketh SJ (2016) Intercomparison and assessment of long-term (2004-2013) multiple satellite aerosol products over two contrasting sites in South Africa. J Atmos Solar Terres Phys 148:82–95

Adesina AJ, Piketh S, Kumar KR, Venkataraman S (2017) Characteristics of columnar aerosol optical and microphysical properties retrieved from the SunPhotometer and its impact on radiative forcing over Skukuza (South Africa) during 1999–2010. Environ Sci Pollut Res 24:16160–16171

Alam K, Thomas T, Thomas B, Hussain M (2012) Aerosol optical and radiative properties during DJF and JJA seasons over Lahore and Karachi. Atmos Environ 50:234–245

Bergstrom RW, Pilewskie P, Russell P, Redemann J, Bond T, Quinn P, Sierau B (2007) Spectral absorption properties of atmospheric aerosols. Atmos Chem Phys 7(23):5937–5943

Bibi H, Alam K, Bibi S (2016) In-depth discrimination of aerosol types using multiple clustering techniques over four locations in indo-Gangetic Plains. Atmos Res 181:106–114. https://doi.org/10.1016/j.atmosres.2016.06.017

Bibi H, Alam K, Bibi S (2017) Estimation of shortwave direct aerosol radiative forcing at four locations on the indo-Gangetic Plains: model results and ground measurement. Atmos Environ 163:166–181

Boiyo R, Kumar KR, Zhao T (2018) Optical, microphysical, and radiative properties of aerosols over a tropical rural site in Kenya, East Africa: source identification, modification and aerosol type discrimination. Atmos Environ 177:234–252

Boiyo R, Kumar KR, Zhao T, Guo J (2019) A 10-year record of aerosol optical properties and radiative forcing over three environmentally distinct AERONET sites in Kenya East Africa. J Geophys Res-Atmos. https://doi.org/10.1029/2018JD029461

Charlson RJ, Schwartz SE, Hales JM, Cess RD, Coakley JA, Hansen JE, Hofmann DJ (1992) Climate forcing by anthropogenic aerosols. Science 255:423–430. https://doi.org/10.1126/science.255.5043.423

Che HZ, Zhang XY, Chen HB, Damiri B, Goloub P, Li XC, Zhang YW et al (2009) Instrument calibration and aerosol optical depth validation of the China aerosol remote sensing network. J Geophys Res-Atmos 114:1–2

Che H, Zhao H, Wu Y, Xia X, Zhu J, Wang H, Wang Y, Sun J, Yu J, Zhang X, Shi G (2015) Analyses of aerosol optical properties and direct radiative forcing over urban and industrial regions in Northeast China. Meteorog Atmos Phys 127:345–354

Che H, Xia X, Zhao H, Dubovik O, Holben BN, Goloub P et al (2019) Spatial distribution of aerosol microphysical and optical properties and direct radiative effect from the China Aerosol Remote Sensing Network. Atmos Chem Phys 19:11843–11864

Derimian Y, Karnieli A, Kaufman YJ, Andreae MO, Andreae TW, Dubovik O et al (2008) The role of iron and black carbon in aerosol light absorption. Atmos Chem Phys 8:3623–3637

Eck TF, Holben BN, Reid JS, Dubovik O, Smirnov A, O'Neill NT, Slutsker I, Kinne S (1999) Wavelength dependence of the optical depth of biomass burning urban and desert dust aerosols. J Geophys Res 104(D24):31333–31349

El-Metwally M, Alfaro SC, Wahab MMA, Favez O, Mohamed Z, Chatenet B (2011) Aerosol properties and associated radiative effects over Cairo (Egypt). Atmos Res 99:263–276

Giles DM, Holben BN, Eck TF, Sinyuk A, Smirnov A, Slutsker, et al (2012) An analysis of AERONET aerosol absorption properties and classifications representative of aerosol source regions. J Geophys Res 117, https://doi.org/10.1029/2012JD018127

Gobbi GP, Kaufman YJ, Koren I, Eck TF (2007) Classification of aerosol properties derived from AERONET direct sun data. Atmos Chem Physics Discuss 6:8713–8726

Hersey SP, Garland R, Crosbie E, Shingler T, Sorooshian A, Piketh S, Burger R (2015) An overview of regional and local characteristics of aerosols in South Africa using satellite, ground, and modeling data. Atmos Chem Phys 15:4259–4278

Holben BN, Eck TF, Slutsker I, Tanré D, Buis JP, Setzer A, Vermote JA, Reagan JA, Kaufman YJ, Nakajima T, Jankowiak I, Smirnov A (1998) AERONET-A federated instrument network and data archive for aerosol characterization. Remote Sens Environ 66:1–16

IPCC. 2013. Climate change 2013: the physical science basis: contribution of Working Group I to the Fifth Assessment Report of the Intergovernmental Panel on Climate Change, Stocker TF, Qin D, Plattner GK, Tignor M, Allen SK, Boschung J, Nauels A, Xia Y, Bex V, Midgley PM. (Eds). Cambridge University Press, Cambridge and New York, pp. 1535

Kang N, Kumar KR, Yu X, Yin Y (2016) Column-integrated aerosol optical properties and direct radiative forcing over the urban-industrial megacity Nanjing in the Yangtze River Delta, China. Environ Sci Pollut Res 23:17532–17552

Kaskaoutis DG, Kambezidis HD, Hatzianastassiou N, Kosmopoulos PG, Badarinath KVS (2007) Aerosol climatology: dependence of the angstrom exponent on wavelength over four AERONET sites. Atmos Chem Phys Discuss 7:7347–7397

Kaskaoutis DG, Kharol SK, Sinha PR, Singh RP, Kambezidis HD, Rani Sharma A, Badarinath KVS (2011) Extremely large anthropogenic-aerosol contribution to total aerosol load over the Bay of Bengal during winter season. Atmos Chem Phys 11:7097–7117. https://doi.org/10.5194/acp-11-7097-2011

Katsanos D, Bougiatioti A, Liakakou E, Kaskaoustis DG, Stavroulas I, Paraskevopoulou D et al (2019) Optical properties of near-surface urban aerosols and their chemical tracing in a Mediterranean City (Athens). Aerosol Air Qual Res 19:49–70

Kumar KR, Narasimhulu K, Reddy RR, Gopal KR, Reddy LSS, Balakrishnaiah G, Moorthy KK, Babu SS (2009) Temporal and spectral characteristics of aerosol optical depths in a semi-arid region of southern India. Sci Total Environ 407:2673–2688

Kumar KR, Sivakumar V, Reddy RR, Gopal KR, Adesina AJ (2013) Inferring wavelength dependence of AOD and Ångström exponent over a sub-tropical station in South Africa using AERONET data: iInfluence of meteorology, long-range transport and curvature effect. Sci Total Environ 461–462:397–408

Kumar KR, Sivakumar V, Yin Y, Reddy RR, Kang N, Diao Y, Yu X et al (2014a) Long-term (2003-2013) climatological trends and variations in aerosol optical parameters retrieved from MODIS over three stations in South Africa. Atmos Environ 95:400–408. https://doi.org/10.1016/j.atmosenv.2014.07.001

Kumar KR, Sivakumar V, Reddy RR, Gopal KR, Adesina AJ (2014b) Identification and classification of different aerosol types over a subtropical rural Site in Mpumalanga, South Africa: seasonal variations as retrieved from the AERONET Sunphotometer. Aerosol Air Qual Res 14(1):108–123

Kumar KR, Yin Y, Sivakumar VN, Yu X, Diao Y, Adesina AJ, Reddy RR (2015) Aerosol climatology and discrimination of aerosol types retrieved from MODIS, MISR and OMI over Durban (29.88°S, 31.02°E), South Africa. Atmos Environ 117:9–18

Kumar KR, Kang N, Sivakumar V, Griffith D (2017) Temporal characteristics of columnar aerosol optical properties and radiative forcing (2011-2015) measured at AERONET's Pretoria_CSIR_DPSS site in South Africa. Atmos Environ 165:274–289

Lee J, Kim J, Song CH, Kim SB, Chun Y, Sohn BJ, Holben BN (2010) Characteristics of aerosol types from AERONET sunphotometer measurements. Atmos Environ 44:3110–3117

Patel PN, Dumka UC, Kaskaoutis DG, Babu KN, Mathur AK (2017) Optical and radiative properties of aerosols over Desalpar, a remote site in western India: source identification, modification processes and aerosol type discrimination. Sci Total Environ 575:612–627

Piketh S, Annegarn H, Tyson P (1999) Lower tropospheric aerosol loadings over South Africa: the relative contribution of aeolian dust, industrial emissions, and biomass burning. J Geophys Res-Atmos 104(D1):1597–1607

Queface AJ, Piketh SJ, Eck TF, Tsay S-C, Mavume AF (2011) Climatology of aerosol optical properties in Southern Africa. Atmos Environ 45(17):2910–2921

Ramanathan V, Crutzen PJ, Kiehl JT, Rosenfeld D (2001) Aerosols, climate, and the hydrological cycle. Science. 294:2119–2124. https://doi.org/10.1126/science.1064034

Ricchiazzi P, Yang S, Gautier C, Sowle D (1998) SBDART: a research and software tool for plane-parallel radiative transfer in the Earth's atmosphere. Bull Am Meteorol Soc 79:2101–2114

Rosenfeld D (2000) Suppression of rain and snow by urban and industrial air pollution. Science 287:1793–1796. https://doi.org/10.1126/science.287.5459.1793

Russell P, Bergstrom R, Shinozuka Y, Clarke A, DeCarlo P, Jimenez J, Livingston J, Redemann J, Dubovik O, Strawa A (2010) Absorption angstrom exponent in AERONET and related data as an indicator of aerosol composition. Atmos Chem Phys 10(3):1155–1169

Singh RP, Dey S, Tripathi SN, Tare V, Holben B (2004) Variability of aerosol parameters over Kanpur, northern India. J Geophys Res Atmos 109:1–14

Sivakumar V, Tesfaye M, Alemu W, Sharma A, Bollig C, Mengistu G (2010) Aerosol measurements over South Africa using satellite, Sun-photometer and LIDAR. Adv Geosci 16:253

Twomey SA (1977) The influence of pollution on the shortwave albedo of clouds. J Atmos Sci 34:1149–1152

Vachaspati CV, Begam GR, Ahammed YN, Kumar KR, Reddy RR (2018) Characterization of aerosol optical properties and model computed radiative forcing over a semi-arid region, Kadapa in India. Atmos Res 209:36–49

Wang YQ, Zhang XY, Draxler RR (2009) TrajState: GIS based software that uses various statistical analysis methods to identify potential sources from long-term air pollution measurement data. Environ Model Softw 24:938–939

Yu X, Lu R, Kumar KR, Ma J et al (2016) Dust aerosol properties and radiative forcing observed in spring during 2001-2014 over urban Beijing, China. Environ Sci Pollut Res 23:15432–15442

Yu X, Lu R, Liu C, Yuan L, Shao Y, Zhu B, Lei L (2017) Seasonal variations of columnar aerosol optical properties and radiative forcing over Beijing, China. Atmos Environ 166:340–350

Zhu J, Che H, Xia X, Yu X, Wang J (2019) Analysis of water vapor effects on aerosol properties and direct radiative forcing in China. Sci Total Environ 650:257–266